DOI: 10.1002/chem.200600001

Synthesis, Structure and Magnetic properties of Chiral and Nonchiral Transition-Metal Malates

Adel Beghidja,[a, b] Pierre Rabu,*[a] Guillaume Rogez,[a] and Richard Welter*[b]

Abstract: Carboxylate-bridged complexes of transition metals, $M^{II}=Mn^{II}$, Fe^{II}, Co^{II}, Ni^{II}, Zn^{II}, were synthesised by reaction of M^{II} salts with DL-malate and L-malate under hydrothermal conditions. These complexes form four series of compounds, which have been fully characterised structurally, thermally and magnetically. The crystal structures of the new chiral compounds, [Mn(L-mal)(H_2O)] (**1**), [Fe(L-mal)(H_2O)] (**2**), [Co(L-mal)(H_2O)] (**3**) and [Zn(L-mal)(H_2O)] (**4**) as well as those of the bimetallic analogues [$Mn_{0.63}Co_{0.37}$(L-mal)(H_2O)] (**5**) and [$Mn_{0.79}Ni_{0.21}$(L-mal)(H_2O)] (**6**) have been solved by single-crystal X-ray diffraction. The six L-malate monohydrates crystallise in the chiral space group $P2_12_12_1$ and consist in a three-dimensional network of metal(II) centres in octahedral sites formed by oxygen atoms. These structures were compared to those of the chiral trihydrate compounds [Co(L-mal)(H_2O)]·2H_2O (**7**), [Ni(L-mal)(H_2O)]·2H_2O (**8**) and [$Co_{0.52}Ni_{0.48}$(L-mal)(H_2O)]·2H_2O (**9**), which exhibit helical chains of M^{II} centres, and those of DL-malate dihydrates [Co(DL-mal)(H_2O)]·H_2O (**10**) and [Ni(DL-mal)(H_2O)·H_2O (**11**) and trihydrate [Mn(L-mal)(H_2O)]·2H_2O (**12**) highlighting the great flexibility of the coordination by the malate ligand. UV/Vis spectroscopic results are consistent with octahedral coordination geometry of high-spin transition-metal centres. Extensive magnetic characterisation of each homologous series indicates rather weak coupling interaction between paramagnetic centres linked through carboxylate bridges. Curie-like paramagnetic, antiferromagnetic, ferromagnetic or weak ferromagnetic behaviour is observed and discussed on the basis of the structural features. The bimetallic compounds **5** and **6** represent new examples of chiral magnets.

Keywords: carboxylate ligands · chiral compounds · hydrothermal synthesis · magnetic properties · transition metals

Introduction

Carboxylate complexes have been much investigated over the last years due to their interesting coordination chemistry allowing for unusual structural features and leading to various physical and chemical properties and practical applications in fields such as dyes, extractants, drugs, pesticides and catalysts.[1–7] Although a great number of carboxylate-based coordination compounds have been obtained to date, the rational design and synthesis of novel metal carboxylates by employing new synthetic tools, varying the nature of the reactants and synthetic conditions, are currently under active investigation.[8–11] Metal carboxylates are also suitable for the design of low-dimensional magnetic systems with outstanding properties.[12–19] In this field, the design of chiral magnetic systems is of particular interest for fundamental investigations on the magneto-chiral effect because of possible applications in magneto-optical devices. However, only few optically active magnets have been reported to date.[20–25] For this purpose, α-hydroxycarboxylic acids, exhibiting a variety of coordination abilities and the tendency to form architectures with multidimensional frameworks, are appealing ligands for building simple new chiral coordination compounds.[26–29] We have recently reported a series of manganese(II), cobalt(II), nickel(II), copper(II) and iron(II) mandelate compounds that show a layered structure and are good examples of two-dimensional (2D) magnetic systems with various magnetic exchange interactions (man-

[a] Dr. A. Beghidja, Dr. P. Rabu, Dr. G. Rogez
Institut de Physique et Chimie des Matériaux de Strasbourg
UMR 7504 CNRS-ULP, 23 rue du Loess
67034 Strasbourg Cedex 2, (France)
Fax: (+33) 3-8810-7247
E-mail: pierre.rabu@ipcms.u-strasbg.fr

[b] Dr. A. Beghidja, Prof. R. Welter
Laboratoire DECOMET, LC003 7177 CNRS-ULP
ILB, Université Louis Pasteur
4, rue Blaise Pascal, 67000 Strasbourg (France)
Fax: (+33) 3-9024-1229
E-mail: welter@chimie.u-strasbg.fr

Supporting information for this article is available on the WWW under http://www.chemeurj.org/ or from the author.

delate = 2-hydroxyphenylethanoate).[30] The 2D character in that case results from the stacking of the phenyl moieties of the mandelate ligands. As for the chirality however, attempts for stabilising pure enantiomers were unsuccessful due to racemisation occurring during the synthesis, preventing the possibility of building a chiral magnetic system on the basis of the mandelate ligands.

Herein, we extend these studies to explore the interactions of malate ligands with transition-metal ions pursuing the aim of designing new chiral compounds exhibiting various architectures and magnetic ordering (malate = hydroxybutanedioate). It is worth noting that several transition-metal malates without another ligand have already been reported in the literature. As for the compounds synthesised by using the racemic mixture of the ligand, cobalt DL-malate dihydrate (**10**), nickel DL-malate dihydrate (**11**) and one mixed metal analogue were reported very recently and exhibit similar structures with a three-dimensional (3D) metal(II) network.[31] The magnetic susceptibilities measured down to 2 K under a 0.5 T applied field were fit to the Curie–Weiss law. Negative and positive Weiss temperatures were found for the Co^{II} and Ni^{II} compounds and these θ values were attributed to antiferromagnetic and ferromagnetic coupling, respectively, between metal centres. It is worth mentioning that this interpretation neglects the possible effect of spin-orbit coupling for Co^{II} ions[32,33] and moreover, other authors reported in very recent work the presence of antiferromagnetic coupling in the Ni^{II} compound **11** on the basis of the observation of a peak of the $\chi T(T)$ curve around 4 K for measurements carried out under a 1 T applied field.[34] The synthesis under normal conditions of Mn DL-malate trihydrate (**12**) was also reported; it exhibits a 2D structure of interconnected $Mn^{II}O_6$ octahedra.[35,36] The magnetic behaviour has not been investigated to date. As for polymeric compounds involving a pure enantiomer, to our knowledge, few metal L-malates have been obtained through normal synthetic routes and characterised.[37–40] Single-crystal structures were reported for the two isostructural Co^{II} and Ni^{II} L-malate trihydrates (**7** and **8**, respectively), which consists of packed chains of interconnected metal–O_6 octahedra.[38,39] In addition, the Mn^{II} L-malate trihydrate crystallises as an extensive polymeric network with a different structure compared to the precedent Ni^{II} and Co^{II} parent compounds.[37,40] To our knowledge, the magnetic behaviours of these three transition-metal malate trihydrates have not been investigated.

In this paper we report on the synthesis by solvothermal routes, the crystal structures and the magnetic characterisation of six new metal(II) chiral compounds with the L-malic acid (**1**–**6**). Their structural features and magnetic behaviours were carefully analyzed and compared to that observed for other members of the series cited above. For other members of the series, single crystals were grown and structures re-determined, except for the Mn L-malate trihydrate, which we did not obtain by hydrothermal synthesis. The behaviours of compounds **10** and **11** have been clarified. Compound **9** has been fully characterised. The magnetic behaviour of compounds **7**, **8** and **12** was investigated for the first time.

Results and Discussion

Synthesis: All the compounds reported here were synthesised by means of solvothermal reactions of transition-metal chlorides or sulfates (1 mmol) with malic acid (0.916 g, 1.5 mmol) and KOH (0.518 g, 2 mmol) in a water and ethanol mixture (50:50 v/v, 5 mL), heated at 180 °C for 48 h in 17 mL Teflon-walled sealed reactor. Six chiral transition-metal malates, $[M(C_4H_4O_5)(H_2O)_n]\cdot n'(H_2O)$ (compounds **1**–**6** with M = Mn, Fe, Co, Ni, Zn, $n = 1$ or 2, and $n' = 0$ or 1) were obtained (see the Experimental Section). The compounds were typically isolated as well-shaped single crystals. The manganese, iron and zinc chlorides and the cobalt sulfate lead to the monohydrate compounds **1**, **2**, **3** and **4**, while the use of the nickel or cobalt chlorides stabilised trihydrate malates. Interestingly, in the case of manganese and nickel, the same compounds were obtained starting from the sulfate salts. The possible influence of the choice of the starting anion, that is, chloride or sulfate, seems thus specific to the cobalt(II) case.

The chemical formulae of the products were ascertained by a set of complementary analytical techniques (elemental chemical analysis, thermogravimetry) demonstrating the consistency of the whole series of samples. As for the mixed compounds **5**, **6** and **9**, the relative amount in metal ions was evaluated by mean of inductive coupled plasma atomic emission spectroscopy (ICP-AES, Liberty 220 Varian Spectrometer, LCAM, ECPM, Strasbourg, France). In addition, information on the structural features of all species was supplied by FT-IR and UV/Vis/NIR spectroscopy, which suggested the presence of hydrogen bonds, of coordinated carboxylate and alcoholic groups and of M^{II} atoms of nearly octahedral coordination geometry (see hereafter). These analytical results as a whole were fully confirmed by single-crystal X-ray diffraction (XRD) studies, discussed below.

Crystal structures

Crystal structures of the L*-malate monohydrates **1**–**6***: The new chiral compounds **1**, **2**, **3** and **4** were obtained as rectangular platelets (see Experimental Section). They are isostructural and crystallise in the chiral orthorhombic space group $P2_12_12_1$. The two new mixed compounds $[Mn_{0.63}Co_{0.37}$-(L-Mal)$(H_2O)]$ (**5**) and $[Mn_{0.79}Ni_{0.21}$(L-Mal)$(H_2O)]$ (**6**) were also obtained as single crystals with the same crystal structure. The cell parameters of the compounds are presented in Table 1.

The solid-state structure of these compounds (**1**–**6**) corresponds to a 3D coordination network of interconnected $M^{II}O_6$ octahedra. The asymmetric unit contains one independent M^{II} ion. As shown in Figure 1a, each metal centre ($M^{II} = Mn^{II}$, Fe^{II}, Co^{II}, Zn^{II}, Mn/Co, Mn/Ni) is surrounded by six oxygen atoms forming a distorted octahedral site. Five

Table 1. Crystal parameters of the first raw transition-metal malates.

Compounds	Space group	a [Å]	b [Å]	b [Å]	β [°]	V [Å^3]	References
Mn L-malate trihydrate	$P2_12_12_1$	*9.219(7)*	*9.421(6)*	*10.536(7)*	–	*915.1(8)*	[37,40]
Mn L-malate monohydrate (**1**)	$P2_12_12_1$	7.988(5)	8.998(5)	9.029(5)	–	649.0(7)	this work
Fe L-malate monohydrate (**2**)	$P2_12_12_1$	7.860(1)	8.923(1)	8.984(1)	–	630.09(13)	this work
Co L-malate monohydrate (**3**)	$P2_12_12_1$	7.754(1)	8.875(1)	8.987(1)	–	618.46(13)	this work
Zn L-malate monohydrate (**4**)	$P2_12_12_1$	7.777(5)	8.882(5)	8.933(5)	–	617.0(6)	this work
$Mn_{0.63}Co_{0.37}$ L-malate monohydrate (**5**)	$P2_12_12_1$	7.881(5)	8.942(5)	8.996(5)	–	634.0(6)	this work
$Mn_{0.79}Ni_{0.21}$ L-malate monohydrate (**6**)	$P2_12_12_1$	7.902(5)	8.942(5)	9.053(5)	–	639.7(6)	this work
Co L-malate trihydrate (**7**)	$P2_1$	5.777(5)	9.079(5)	8.411(5)	105.433(5)	425.2(5)	this work
	$P2_1$	5.789(2)	9.062(10)	8.450(6)	105.42(4)	427.3(5)	[38]
Ni L-malate trihydrate (**8**)	$P2_1$	5.753(5)	8.990(5)	8.380(5)	105.523(5)	417.6(5)	this work
	$P2_1$	5.7574(9)	8.990(2)	8.396(2)	105.54(2)	418.7(3)	[39]
$Co_{0.52}Ni_{0.48}$ L-malate trihydrate (**9**)	$P2_1$	5.773(5)	9.047(5)	8.419(5)	105.478(5)	423.8(5)	this work
Co DL-malate dihydrate (**10**)	Cc	13.174(5)	7.536(5)	9.750(5)	130.755(5)	733.2(7)	this work
	Cc	13.211(3)	7.564(2)	9.758(2)	130.83(3)	737.7(3)	[31,34]
Ni DL-malate dihydrate (**11**)	Cc	13.104(5)	7.509(5)	9.633(5)	130.898(5)	716.5(7)	this work
	Cc	13.103(3)	7.526(2)	9.629(2)	130.88(3)	718.0(2)	[31,34]
Mn DL-malate trihydrate (**12**)	$Pbca$	8.266(5)	14.203(5)	14.646(5)	–	1719.5(13)	this work
	$Pbca$	8.265(5)	14.201(8)	14.656(4)	–	1720.2(5)	[35,36]

oxygen atoms are provided by four different malate ligands (O1–O5) and the sixth one is provided by a water molecule (O6). The oxygen atoms provided by the organic ligands belong to the carboxylate group, except for the O3 atom, which belongs to a hydroxy group in α-position. Each metal centre is connected by four neighbouring M^{II} ions through carboxylate bridges with two different metal–metal distances, d_{M-M} being 5.23/5.39, 5.25/5.33, 5.25/5.30 and 5.20/5.28 Å for compounds **1**–**4**, respectively. The octahedral sites are distorted in the four structures with the angles O2-Mn-O5 = 155.5°, O2-Fe-O5 = 158.3°, O2-Co-O5 = 161.2°, O2-Zn-O5 = 158.8°. The metal–oxygen distances are of similar order of magnitude in the four compounds in the range 2.04–2.17 Å for the M−O(malate) bonds and 2.23–2.30 Å for the M−O-(water). Figure 2a shows the 3D network of octahedra in the crystal structure.

The structures of the compounds **7**, **8** and **10**–**12**, obtained as single crystals by the hydrothermal route, were re-examined for comparison with that of the precedent new series of chiral malates.

Crystal structure of the L*-malate trihydrates (**7**–**9**)*: The compounds **7** and **8** crystallised as dark pink platelets for the cobalt derivative (**7**) and green platelets for the nickel analogue (**8**). The new mixed compound **9** is dark pink. The three compounds have similar crystal cells (see Table 1) with the chiral monoclinic space group $P2_1$. The structure shown in Figures 1b and 2b is composed of quasi-isolated helical chains (packed along c) of metal ions coordinated by malate ligands and water molecules. The chains are based on interconnected octahedra formed by central metal(II) ions surrounded by six oxygen atoms: O1, O2, O3 from one ligand, O5 belonging to a second malate, and the slightly distorted octahedron being completed by two water molecules in *cis* positions. A third crystallisation water molecule is present in the asymmetrical unit, but is not coordinated to the metal centre. Within the chains, the octahedra are connected through carboxylato bridges with nearest-neighbour metal–metal distances of 5.32 and 5.25 Å for the Co^{II} and Ni^{II} ions, respectively. No ordering between the two metal ions could be observed by single-crystal X-ray diffraction in the mixed compound **9**.

Crystal structure of the DL*-malate dihydrates (**10** and **11**)*: The compounds **10** and **11** were obtained by using the racemic mixture (DL). Their crystal structures are centro-symmetrical (monoclinic, space group *Cc*, see Table 1), and the metal centres M^{II} (Co^{II}, Ni^{II}) lie in distorted octahedral environments coordinated by three different malate ligands and one water molecule (Figure 1c). The metal–oxygen octahedra are interconnected in the three directions of space, forming a 3D network (Figure 2c) in which each metal ion is linked to four other metal centres, each exchange pathway made up of one carboxylato bridge (O1-C1-O2) and one longer bridge involving two or three carbon atoms (O3-C2-C1-O2 or O3-C2-C3-C4-O5). The distances between two neighbouring metal ions are 5.27 and 5.33 Å for cobalt, and 5.22 and 5.28 Å for the nickel compound.

Crystal structure of the Mn DL*-malate trihydrate (**12**)*: The crystal structure of the manganese DL-malate trihydrate is orthorhombic with the space group *Pbca* (see Table 1). The structure is formed of distorted $Mn^{II}O_6$ octahedra interconnected by the D- and L-malate molecules in a *trans*-conformation. Around the Mn^{II} centres, the oxygen atoms O1 and O3 belong to one malate, O4 to a second malate and O5 to a third one. The coordination sphere is completed by two water molecules (O6, O7) leading to a distorted octahedron

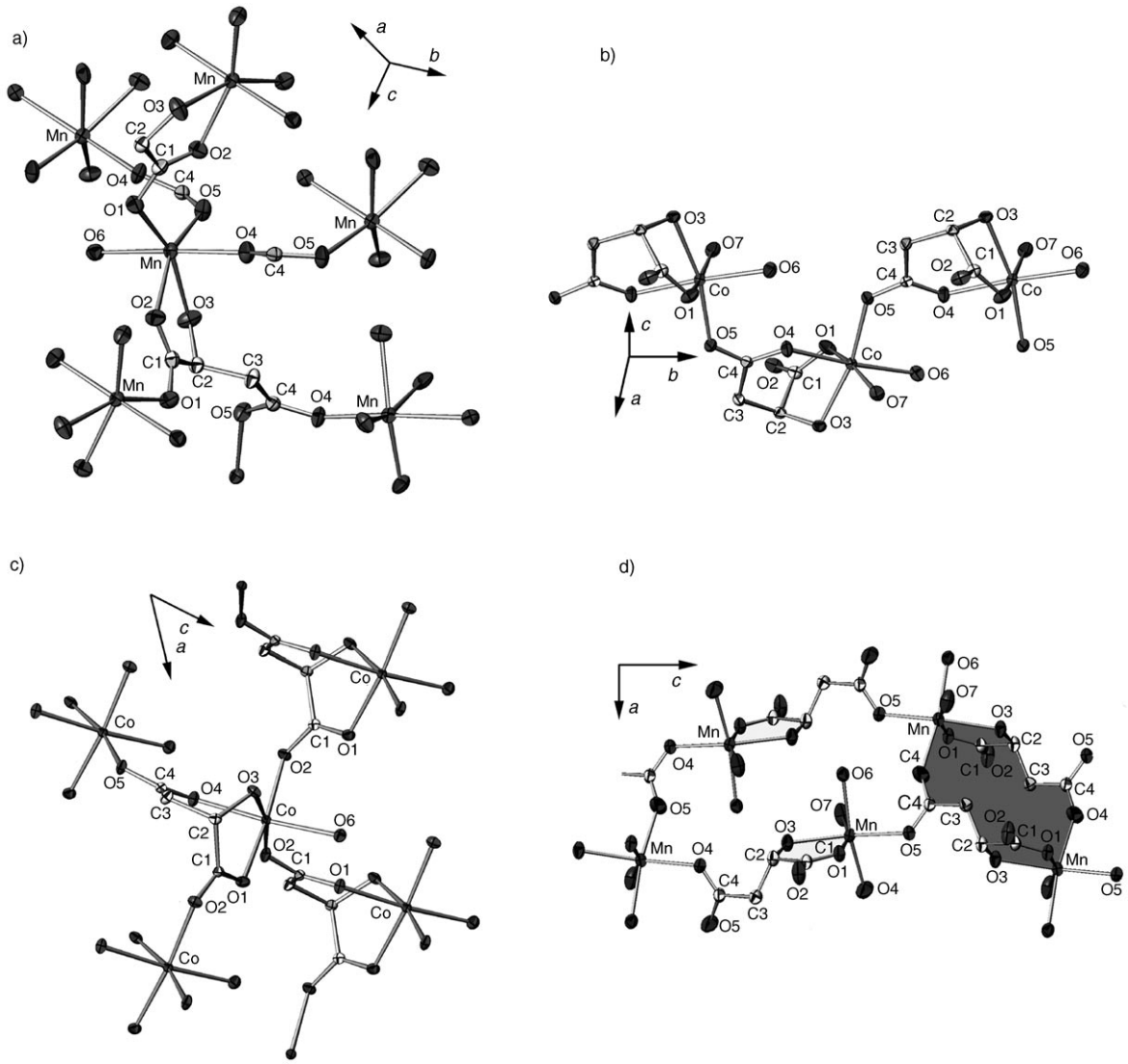

Figure 1. Crystal structures of compounds a) **1**, b) **7**, c) **10** and d) **12**. H atoms and unbounded solvent H_2O molecules have been omitted for clarity. Only atoms around the metal centre have been labelled. Thermal ellipsoids enclose 50% of the electronic density.

(O3-Mn-O5 = 159.7°). There is a third water molecule that is not linked to the metal ions. The octahedra form pseudolayers of 20- and 13-membered rings, containing four and two Mn atoms, respectively, parallel to the (1 0 0) crystallographic planes (see Figure 1d and Figure 2d). The Mn^{II} ions in the 13-membered rings (shaded in Figure 1d) are linked by a malate ligand, whereas in the 20-membered rings they are connected by alternate malate (O1-C1-C2-C3-C4-O4) and carboxylate (O4-C4-O5) bridges. Compound **12** is the only one in the series that we obtained crystallising in this structure.

The different structural features are summarised in the Scheme 1. Depending on the starting metal salt, and the enantiomeric purity of the carboxylate, different coordination modes of the malate ligand were observed. We obtained four types of structures, two chiral structures with the L enantiomer and two nonchiral structures with the racemic mixture, corresponding to four different modes of coordination to the metal and resulting in different topologies of the magnetic networks, stabilised by the presence of 1–3 water molecules in the asymmetrical unit.

Thermogravimetric analysis: The thermal stability of the compounds was evaluated by thermogravimetric analysis between ambient temperature and 700 °C in air (see Figure S1 in the Supporting Information). The four isostructural products **1**–**4** were observed to lose their water molecules at around 250 °C and to decompose in the range 320 °C–430 °C, the decomposition temperature increasing with the atomic number. As for the L-malate trihydrate structure, compounds **7** and **8** started to decompose at 100 and 120 °C, respectively. After loosing their water molecules, cobalt and nickel oxides were obtained at 380 °C. The DL-malate dihydrates **10** and **11** decomposed to oxides at 370 °C, after a

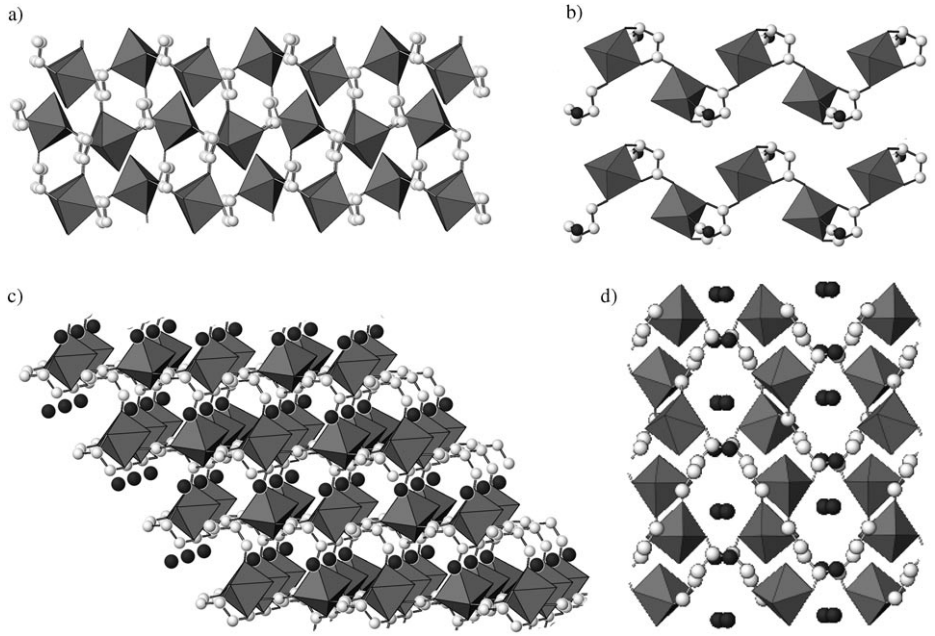

Figure 2. Perspective view of the crystal structures of a) L-malate monohydrates (**1**–**6**), b) L-malate trihydrates (**7**–**9**) in the *bc* plane, c) DL-malate dihydrates (**10** and **11**) in the *ac* plane and d) Mn DL-malate trihydrate (**12**) in the *bc* plane.

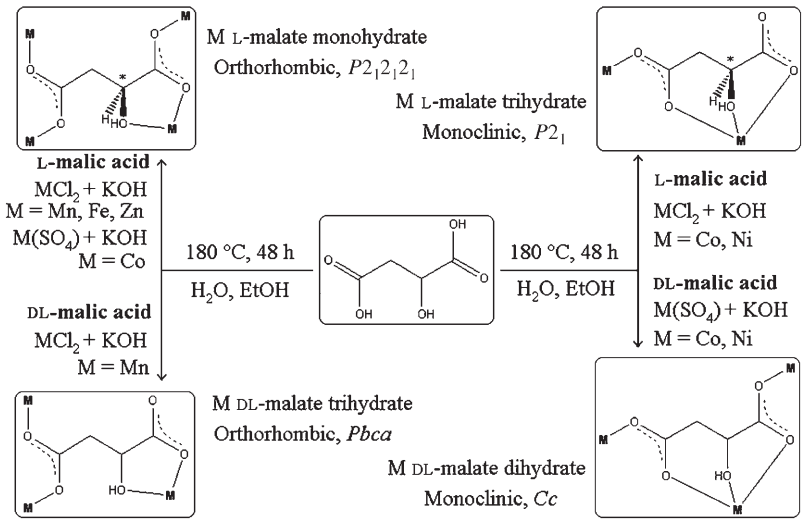

Scheme 1. Coordination modes and crystal structure space groups of transition-metal malates.

water loss occurring in two steps at around 220 and 300 °C. Finally, compound **12** lost the three water molecules successively at 134, 176 and 303 °C, and decomposed in oxide at approximately 360 °C. It is worth noting that all the compounds exhibit a very exothermic decomposition, leading to an overflow of the temperature regulation.

Spectroscopic properties: The IR and UV/Vis data collected for all compounds (see Experimental Section) are consistent with their crystal structures. The IR spectra clearly exhibit bands characteristic of the malate ligand. Concerning the carboxylate moieties, the frequency differences between the symmetrical and antisymmetrical C–O vibrations ($\Delta\nu$ = 93–152 cm^{-1}) are all much smaller than that observed with the corresponding acid ($\Delta\nu_a$ = 299 cm^{-1}) as required by the coordination modes of the carboxylic groups.[41] The characteristic band for the C–O vibration of the alcoholic group of the malate anions was observed at about 1100 cm^{-1}. The presence of one, two or three broad νO–H bands in the range 3048–3500 cm^{-1} for the series of compounds is related to the aqua ligands implicated in hydrogen bonds. Indeed, the presence of classical hydrogen bonds have been detected in all crystal structures, thus bearing out the role these bonds play in the cohesion of the structures. For example, the Figure 3 shows the diversity of such interactions in compound **1**. They are associated in particular with the water molecules (O6 or O7). All these hydrogen bonds, determined by the PLATON software, are listed in Table S3 in the Supporting Information. The absorption band observed at 1614–1653 cm^{-1} is typical of the bending vibration mode of water molecules strongly bonded to the metal centres.

The UV spectra of all the compounds corroborate the quasi-octahedral geometry of the M^{II} ions.[42,43] The values of Dq and Racah's parameter B for the Co^{II} and Ni^{II} compounds were estimated from the observed absorption bands given in Table 2 and are reported in Table 3.[44] They indicate a low crystal field ($Dq/B \approx 0.93$–1.13) that is consistent with high-spin configuration of the metal(II) centres, in agreement with the magnetic findings (see below). Unlike the three nickel compounds exhibiting very similar absorption bands, the cobalt(II) compounds show different spectra, especially **3** with respect to the other analogues **7** and **10**. This is merely due to different distortions of the coordina-

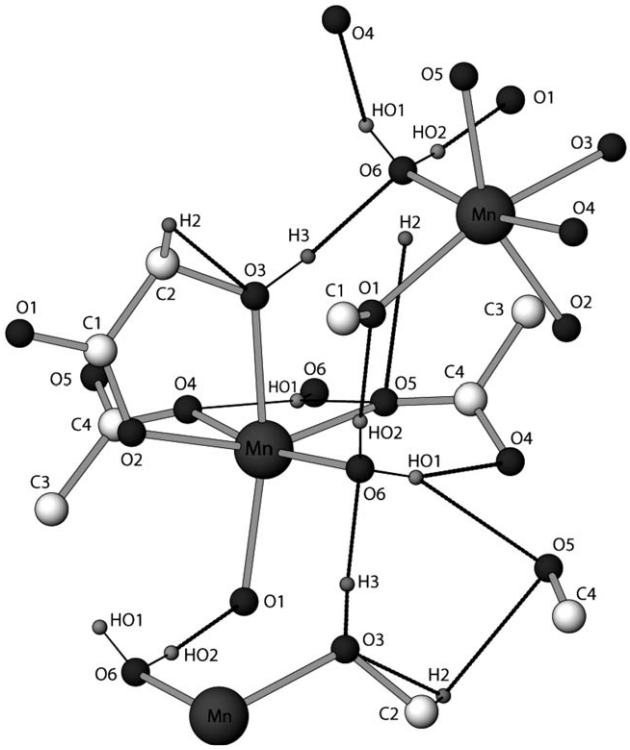

Figure 3. Partial view of the crystal structure of compound **1** showing the classical hydrogen bonds (for details, see Table S3 in the Supporting Information).

Table 2. Assignments of UV/Vis/NIR absorption bands [cm^{-1}] of the cobalt and nickel compounds.

Frequency assignments	**3**	**7**	**10**
ν_1: $^4T_{1g}(F)\rightarrow{}^4T_{2g}(F)$	7550	8440	8200
ν_2: $^4T_{1g}(F)\rightarrow{}^4A_{2g}(F)$	15000	16700	16500
ν_3: $^4T_{1g}(F)\rightarrow{}^4T_{1g}(P)$	18700	19800	19400
Frequency assignments	**8**	**11**	
ν_1: $^3A_{2g}(F)\rightarrow{}^3T_{2g}(F)$	8740	8660	
ν_2: $^3A_{2g}(F)\rightarrow{}^3T_{1g}(F)$	13600	13550	
ν_3: $^3A_{2g}(F)\rightarrow{}^3T_{1g}(P)$	25400	25500	

Table 3. Values of Dq and B calculated from experimental ν_1 and ν_3 values for the Co^{II} and Ni^{II} compounds.[44]

	Dq [cm^{-1}]	B [cm^{-1}]	Dq/B
$^4T_1$ ground state			
ν_1, ν_2	$[(5\nu_3^2-(\nu_3-\nu_1)^2)^{1/2}-2(\nu_3-2\nu_1)]/40$	$(\nu_3-2\nu_1+10\,Dq)/15$	–
3	830	790	1.04
7	920	810	1.13
10	900	800	1.12
$^3A_2$ ground state			
ν_1, ν_3	$\nu_1/10$	$(\nu_3-2\nu_1)\ (\nu_3-\nu_1)/(3(5\nu_3-9\nu_1))$	–
8	870	910	0.96
11	870	930	0.93

tion sphere around the central cobalt(II) ion in the three different structures. For the other members of the series, only the iron(II) malate (**2**) exhibits a clear allowed transition ($^5T_{2g}\rightarrow{}^5E_g$) leading to the approximate value $Dq \approx 940\ cm^{-1}$.

To evaluate directly the chirality of the structures of the compounds **1**–**10**, measurements of the UV circular dichroism (CD) in the solid state were carried out by using a JASCO 810 spectrometer on powder samples embedded in KBr pellets.[45] The results obtained for the Co^{II} derivatives **3** and **7**, which exhibit the most effective absorption in the UV-Vis spectral range, are shown in Figure 4. By comparison with the racemic Co^{II} compound **10**, a significant dichroism is observed in the range 450–600 nm that is associated to the Co^{II} centres as shown by the comparison with the UV reflectance spectra in Figure 4.

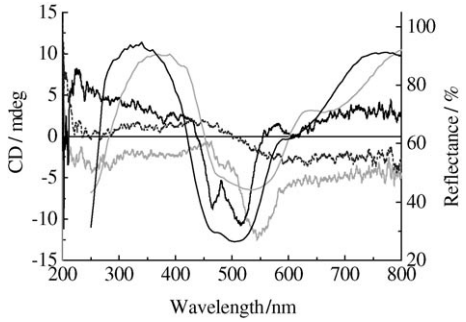

Figure 4. CD spectra of compounds **3** (black) and **7** (grey) compared to their respective UV spectra (same symbols) and to the CD spectrum of the racemic compound **10** (dashed).

This shows that the electronic transitions on the metal ions are sensitive to the polarisation of light. In other words, there was a "transfer" of chirality from the ligand to the magnetic centre. This result is particularly promising in view of observing possible magneto-chiral effects. It is also noticeable that the dichroic signal of the metal consists of two peaks corresponding to a lift of degeneracy associated with a lowering of the symmetry of the cobalt(II) environment with respect to ideal O_h. The variation of the intensities and the position of the two peaks observed between the two chiral compounds are probably due to structural features, the environment around the cobalt being different in **3** and **8**.

Magnetic properties: The magnetic properties of the present series of compounds were investigated on polycrystalline samples. The magnetic susceptibility χ was measured under 500 Oe applied fields, corresponding in all cases to linear variation of M versus H, and suitably corrected for sample and holder diamagnetism. In addition ac susceptibility measurements were performed under a 3.5 Oe ac field at low

temperature to check the occurrence of ferromagnetic ordering.

The main magnetic characteristics of all the series are summarised in Table 4. For all the compounds, the magnetic susceptibilities χ grow smoothly with decreasing temperature down to 4 K (see below). Accordingly, the inverse susceptibilities (not shown) fit the Curie–Weiss law $\chi = C/(T-\theta)$ well at temperatures higher than 200 K. The respective Curie constants reported in Table 4 agree well with those expected for six-coordinated high-spin M^{II} ions.[46]

Table 4. Summary of the magnetic characteristics of transition-metal malates.

	Magnetic behaviour[a]	C [K cm^3 mol^{-1}]	θ [K]	T_C [K]	T_N [K]	M_{sat} [μ_B]
1	3D AF	4.20	−0.23	–	3.5	3.52[b]
2	AF	3.29	14.1	–	–	3.12[b]
3	AF	2.94	−6.00	–	–	2.32
4	DIA	–	–	–	–	–
5	3D wF	3.87	−4.86	≈1.8	–	3.54[b]
6	3D wF	3.71	−6.34	2.31	–	3.67[b]
7	1D F	3.46	−17.8	–	–	2.83
8	1D F	1.30	1.91	–	–	2.28
9	FI	1.98	0.90	–	–	2.51
10	3D F	3.23	−15.3	1.63	–	2.82
11	3D F	1.32	5.76	2.70	–	2.22
12	AF	4.22	−1.71	–	–	4.71[b]

[a] AF: antiferromagnetic, DIA: diamagnetic, wF: weak ferromagnet, F, ferromagnetic, FI: ferrimagnetic, 1D/3D: one/three-dimensional ordering. [b] Values at 5 T, but saturation is not fully reached.

M L-*malate monohydrates (**1–3**, **5–6**)*: Concerning the new chiral three-dimensional compounds **1–3**, various behaviours are observed depending on the metal centres. The magnetic susceptibilities of the three analogues are plotted together with the corresponding χT products in Figure 5. At high temperature, the χT product of the manganese(II) derivative is quasi-constant at 4.20 K cm^3 mol^{-1} and decreases down to 0.69 K cm^3 mol^{-1} at 1.8 K thus denoting antiferromagnetic interactions between Mn^{II} ions,; these interactions are expected to be small according to the small negative Weiss temperature $\theta = -0.23$ K. The magnetic susceptibility exhibits a sharp maximum of 0.36 cm^3 mol^{-1} at $T_N = 3.5$ K, which indicates the occurrence of a long-range antiferromagnetic order. Accordingly, the magnetisation versus field curve at 1.8 K (Figure S2 in the Supporting Information) is characteristic of an antiferromagnet, for which $M(H)$ is small compared to that expected for saturated $S = 5/2$ ions (5 μ_B) and increases slowly with H, showing a slight curvature typical of a spin-flop mechanism.[46]

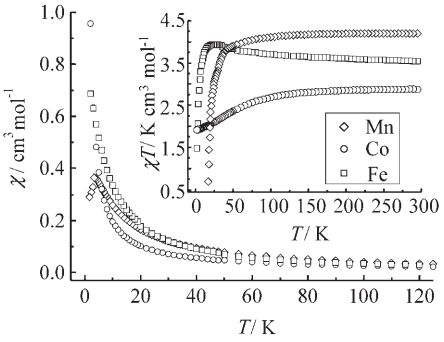

Figure 5. Magnetic susceptibility versus temperature variation for the compounds **1–3**.

The χT product for the Fe^{II} analogue exhibits a upward trend between 3.45 K cm^3 mol^{-1} at 300 K and 3.92 K cm^3 mol^{-1} at 26 K, pointing to the presence of ferromagnetic coupling through carboxylate bridges, as also inferred by the positive Weiss temperature $\theta = 14.1$ K, which is quite large. Below this temperature antiferromagnetic behaviour is observed, characterised by the gradual decrease of χT (1.47 K cm^3 mol^{-1} at 2 K). No long-range order was observed down to 1.8 K, and the $M(H)$ curve shown in Figure S2 in Supporting Information is typical of a paramagnetic phase with a maximum value of the moment of 3.12 μ_B at 5 T tending toward the expected saturation value of 4 μ_B for Fe^{II} $S = 2$ ions.

In the case of the compound **3**, the decay of χT upon cooling, shown in Figure 5, is well explained by the effect of spin-orbit coupling, known to exist for Co^{II} ions,[46,32,33] and which contributes to the lowering of the effective moment of the Co^{II} centres, the observed value of which ($\mu_{eff} = (8\chi T)^{1/2} = 4.8$ and 3.8 μ_B at 300 and 1.8 K, respectively) is consistent with quasi-isolated Co^{II} ions.[32] In addition, the magnetisation curve $M(H)$ shown in Figure S2 in the Supporting Information has the typical shape for a paramagnet and saturates at $M_S = 2.32$ μ_B as expected (2–3 μ_B for Co^{II} ions).[46,32]

Thus the three chiral compounds **1–3** exhibit a paramagnetic behaviour in almost the whole range of temperature, with a tendency to antiferromagnetic coupling. Even though the structure is unchanged, differences are observed; the Co^{II} derivative behaves like quasi-isolated ions, whereas the results for the Fe^{II} analogue indicate the presence of both ferromagnetic and antiferromagnetic interactions through carboxylate bridges between adjacent magnetic centres. The three compounds are characterised by important deviation from the Curie law ($\chi = C/T$) due to efficient short-range interactions, but only the Mn^{II} compound was observed to order antiferromagnetically at a long range below $T_N = 3.5$ K.

The three compounds do not order ferromagnetically, and hence are not chiral magnets. Thus the bimetallic analogues **5** and **6** were synthesised in order to get a ferromagnetic-like state resulting from noncompensation between the moments of interacting centres carrying different spin moments. Indeed, such a ferrimagnetic approach was shown to be successful for the design of magnetic phases on the basis of antiferromagnetic interaction network.[33,47–50] The present compounds are isostructural with the homometallic **1–3** above, as found from their single-crystal X-ray structures. It was not possible, however, to distinguish between Co^{II} and Ni^{II} and Mn^{II} ions owing to very similar X-ray diffusion fac-

tors and no superlattice was evidenced in the structure analysis, as would have resulted from any ordering between the different metal ions. Thus, it was assumed that Co^{II}, Ni^{II} or Mn^{II} are statistically spread over the unique octahedral site of the orthorhombic cell. Such a situation is not favourable for effective unbalancing of spins as shown, for instance, in intercalated MPS_3 (M = Mn, Fe, Ni) series of compounds.[51] Nevertheless, as shown below, the magnetic behaviour of these compounds indicates that some net magnetisation may appear. As reported in Table 4, the Curie constants of compounds **5** and **6** agree with their respective M^{II} contents and the Weiss temperatures are negative revealing antiferromagnetic coupling similarly to the parent homometallic compounds. Indeed, the $\chi T(T)$ curve of the Mn/Co compound **5** (not shown) exhibits a continuous decrease from 3.8 $K cm^3 mol^{-1}$ at 295 K down to 1.25 $K cm^3 mol^{-1}$ at 2 K. Alternative field (ac) susceptibility measurements suggest the upset of an out of phase signal at 1.8 K, but very low temperature data would be necessary for drawing any conclusion on the existence of a 3D ferromagnetic-like ordering in this compound.

As for the Mn/Ni compound **6**, its χT product, shown in Figure 6, behaves similarly to that of **5**. However, an unambiguous upward variation is observed at 2 K. Moreover, a peak in the out of phase signal χ'' of the ac susceptibility is clearly evidenced at low temperature, which is the signature of a 3D ferromagnetic-like ordering. These features are fully confirmed by the magnetisation versus field hysterisis curve recorded at 1.8 K (Figure 7), the shape of which is characteristic of a weak ferromagnet. A small coercive field of approximately 70 Oe is observed.

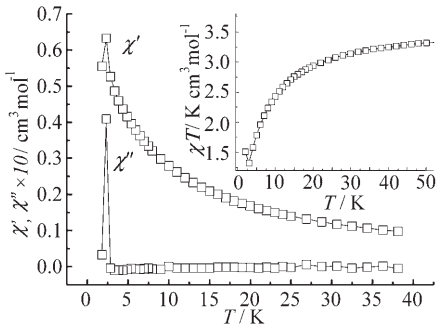

Figure 6. Magnetic susceptibility versus temperature variation for **6** (inset) and ac susceptibility recorded in an alternative field of 3.5 Oe. (Full lines are only guide for the eyes.)

M L-*malate trihydrates (**7**–**9**)*: For comparison with the precedent compounds, we have investigated the magnetic properties of the trihydrate chiral chain compounds **7** and **8**, the magnetic properties of which have not been investigated to date. The magnetic susceptibility of the Co^{II} compound **7** is shown in Figure 8. Starting from high temperature, the χT product slides to a minimum of 2.4 $K cm^3 mol^{-1}$ at 10 K. The fall is typical of the spin-orbit coupling effect (see above).

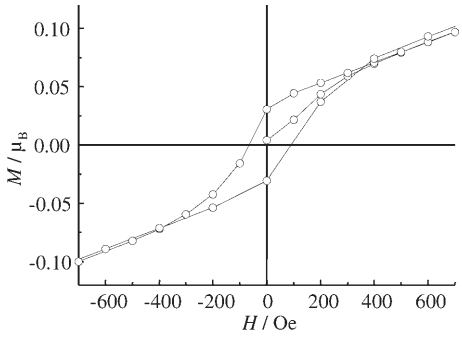

Figure 7. Magnetisation versus field curve at 1.8 K for **6**. (Full line is only guide for the eyes.) The mixed L-malate monohydrates **5** and **6** are new low-temperature chiral magnets.

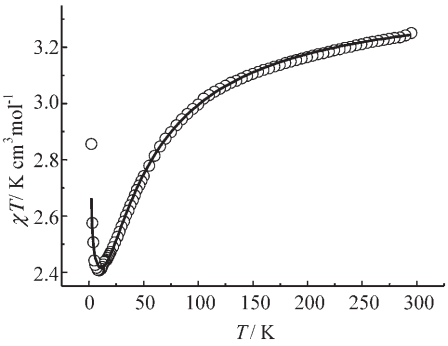

Figure 8. Magnetic susceptibility versus temperature variation for **7**. The solid line corresponds to the fit with the two exponential model described in the text.

Then the upturn of χT toward higher values at relatively low temperature indicates the occurrence of small ferromagnetic interactions within the chains.

Looking at the structure, this ferromagnetic coupling occurs mainly through the carboxylato bridges along the $(\text{-OCO-Co-})_n$ chains, the other pathway by means of the α-hydroxo group, which involves additional C–C bonds, being significantly longer. No analytical expression is available in the literature describing the temperature dependence of χT for chains of Co^{II} ions with spin-orbit coupling. In addition, the low-temperature approximation that involves the treatment of the Co^{II} ions as anisotropic pseudo-spins with $S = 1/2$ below 30 K,[46,33] leading to an Ising-like chain system, is not satisfactory for compound **7**, because the exchange interaction is too weak to show up clearly against the spin-orbit coupling contribution. To get an estimation of the strength of the ferromagnetic exchange interaction, it has been shown previously[52,53] that one may use the simple phenomenological equation:[54–56] $\chi T = A_1 \exp(-E_1/kT) + A_2 \exp(-E_2/kT)$, in which $A_1 + A_2$ equals the Curie constant, and E_1 and E_2 are the "activation energies" corresponding to the spin-orbit coupling and to the ferromagnetic exchange interaction, respectively. This equation describes the spin-orbit coupling, which results in a splitting between discrete levels, and the exponential low-temperature divergence of the susceptibility ($\chi T \propto \exp(+J/2kT)$) of an Ising chain of

anisotropic magnetic centres like Co^{II} at low temperature. The experimental data for **7** have been fit by using a least-square refinement method. This model fits to the experimental data very well for the refined parameters values $A_1 = 1.06(1)\ K\,cm^3\,mol^{-1}$, $E_1/k = +50.5(5)\ K$, $A_2 = 2.35(1)\ K\,cm^3\,mol^{-1}$ and $E_2/k = -0.25(1)\ K$ (Figure 8). The value found for $C = A_1 + A_2 = 3.41(1)\ K\,cm^3\,mol^{-1}$ is similar to the one obtained by using the Curie–Weiss law in the high-temperature range (see Table 4) and the values for E_1/k are consistent with those given in the literature for both the effects of spin-orbit coupling and site distortion in various Co^{II} coordination compounds (E_1/k of the order of 50–100 K).[32,52,53] The ferromagnetic exchange interaction is weak indeed, with the value $-E_2/k = -0.25$ K corresponding to interactions $J = +0.5$ K within the Ising chain approximation. As expected, the exchange coupling is really weak and the carboxylate bridge is not a inefficient exchange pathway.

The temperature variation of the magnetic susceptibility of the Ni^{II} analogue **8** is presented on Figure 9. The χT product exhibits a regular growth with decreasing temperature up to $3.07\ K\,cm^3\,mol^{-1}$ at 2 K, illustrating the occurrence of ferromagnetic coupling within the Ni^{II} chains. The steep increase in the magnetisation with applied field at 2 K confirms the ferromagnetic behaviour; however, no long-range ordering was observed at this temperature.

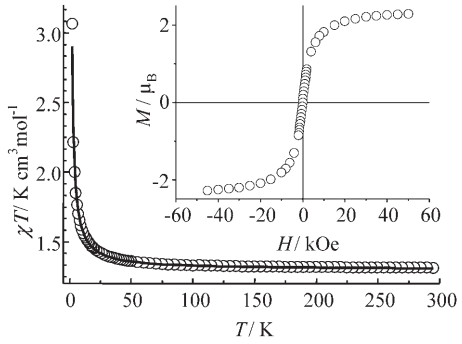

Figure 9. Magnetic susceptibility versus temperature variation for the Ni^{II} chain compound **5**. The solid line corresponds to the fit with the power law model described in the text. The magnetisation versus field variation at 2 K is plotted in the inset.

To evaluate the exchange interaction between neighbouring nickel(II) atoms, the high-temperature susceptibility was fit by using a simple model for Heisenberg $S = 1$ ferromagnetic regular chains, developed within the frame of the scaling theory by Souletie[57–59] and already applied to Ni^{II} and Cu^{II} chains.[56,59,60] In this approach, the zero-field splitting for nickel(II) is not taken into account, assuming that its effect is significant only at low temperature ($T < 16$ K).[61] The spin exchange Hamiltonian of a chain system of spins S ($\hat{H}_{ex} = -J \sum_{i=1}^{N} \hat{S}_i \hat{S}_{i+1} - g\mu_B \sum_{i=1}^{N} \hat{S}_i \vec{H}$) can be solved, numerically, only for ring chains involving a limited number of spins N. The study of the variation of the susceptibility as a function of the temperature, for chains of various size (up to $N = 14$) and for various spins ($S = 1/2$, 1, 3/2) shows that data corresponding to N and $N+1$ chains coincide in a wide range down to a threshold value $T_S(N)$, the value of which decreases as N increases. $T_S(N)$ corresponds to the limit above which the calculation for N spins is the exact solution for the infinite chain maximum. In addition, it was observed that, for given S values, $\partial\log(T)/\partial\log(\chi T) = f(T)$ for finite ferromagnetic rings of N Heisenberg spins is a linear function that intercepts the axes at T_C and γ^{-1} (both negative) that stays much the same for different N values. Consequently the following expression [Eq. (1)] of the susceptibility for the infinite chain was deduced, which holds for $T > T_S(\infty)$ and in which C is the Curie constant ($g^2\mu_B^2 S(S+1)/3k$) and γ is a critical exponent.

$$\chi T = C\,(1 + \Theta J\,S(S+1)/T)^{-\gamma} \quad \text{with } \Theta > 0 \tag{1}$$

The best values of C, Θ and γ, for $S = 1/2$, 1, 3/2, were obtained by fitting the susceptibility data for the largest rings, that is, for $N = 14$ ($S = 1/2$), $N = 10$ ($S = 1$) and $N = 8$ ($S = 3/2$), in the temperature range $T > T_S(N)$. These results enabled to lead to the following simple general expression for χT [Eq. (2)], which is clearly more tractable than the polynomial expressions reported for Heisenberg spins in the literature.[62,63]

$$\chi T = C\,(1 + 0.6J(S+1)/T)^{1.25S} \quad \text{for } T > T_S \tag{2}$$

Finally, this simple expression, with $S = 1$, fits very well the experimental susceptibility of compound **8** (Figure 9), giving $g = 2.28(1)$ and $J/k = +1.50(1)$ K, which is weak and in accordance with the value of θ deduced above (Table 4).

Similarly as above, we synthesised the new mixed Co/Ni compound **9** to stabilise a ferrimagnetic system. The χT versus T curve (not shown) exhibits a typical shape with a decrease from $2.0\ K\,cm^3\,mol^{-1}$ down to a minimum around 20 K followed by a steep increase, in agreement to a ferrimagnetic chain system. However, no long-range ordering was observed in the range 1.8 K–300 K.

M DL*-malate dihydrates (**10** and **11**)*: Magnetic data for the Co^{II} and Ni^{II} DL-malate dihydrates **10** and **11** were already reported in the literature.[31,34] As mentioned in the introduction however, these results were not consistent one with the other. We have thus investigated again the magnetic behaviours of these compounds carrying out careful measurements that were repeated on several polycrystalline samples to check their reliability. In particular, the susceptibility measurements were done under applied fields smaller than 500 Oe, in order to remain in the linear part of the magnetisation versus field curve within the largest temperature range.

The thermal variation of the magnetic susceptibility and the magnetisation versus field curve (recorded at 1.8 K) of the Co^{II} derivative **10** are plotted in Figure 10. First, the value of χT at 300 K is $3.11\ K\,cm^3\,mol^{-1}$, in agreement with the expected value for high-spin Co^{II} ions in octahedral

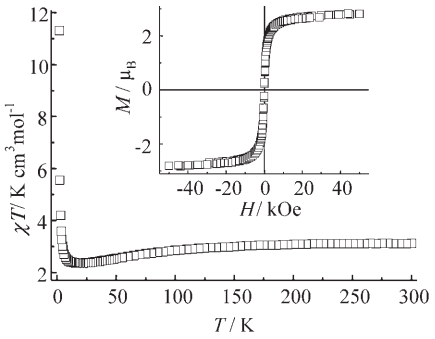

Figure 10. Magnetic susceptibility versus temperature variation recorded under 500 Oe applied field for the Co^{II} compound **10**. The magnetisation versus field variation at 1.8 K is plotted in the inset.

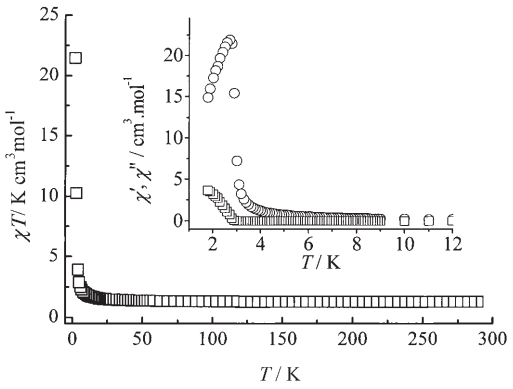

Figure 11. Magnetic susceptibility versus temperature variation recorded under 500 Oe applied field for the Ni^{II} compound **11**. The thermal variation of the real (circles) and out of phase (squares) components of the ac susceptibility recorded in a 3 Oe ac field is plotted in the inset.

sites, as well as the related Curie constant given in Table 4. on lowering the temperature, $\chi T(T)$ decreases to a minimum of 2.35 $K cm^3 mol^{-1}$ around 19 K followed by an abrupt increase up to the relatively high value of 11.32 $K cm^3 mol^{-1}$ at 1.8 K. The decrease at high temperature can be ascribed to spin-orbit coupling effect for Co^{II} ions in octahedral sites. Although weak antiferromagnetic coupling cannot be ruled out, it is worth noting that the minimum value of χT is near that expected for isolated Co^{II} centres as mentioned for compound **3**. The sharp increase at low temperature illustrates the occurrence of ferromagnetic interactions.

Moreover, the magnetisation cycle recorded at 1.8 K exhibits a steep slope at $H=0$ Oe and the saturation value at high field (2.8 μ_B) is very near the maximum value of 3 μ_B expected for three unpaired electrons. All these features suggest a long-range ferromagnetic ordering at very low temperature. This point was inferred by low-temperature specific heat measurements shown in Figure S3 in the Supporting Information. Below 2 K $Cp(T)$ diverges and reach a maximum of 13 $J mol^{-1} K^{-1}$ at the Curie temperature $T_C=$ 1.64(1) K. Thus, in contrast to what was presumed in reference [31], the Co^{II} compound behaves really as a ferromagnet.

Concerning the Ni^{II} analogue, the χT product (Figure 11) increases with decreasing temperature, consistently with the results reported in reference [31] and [34], excepted that no maximum is observed under low applied field.

As shown in Figure S4 in the Supporting Information, the magnetisation versus field cycle measured at 1.8 K is characteristic of a ferromagnetic ordering, the saturation value of 2.2 μ_B indicating a full alignment of the $S=1$ spin moments. In fact the measurements interpreted in reference [34] were done under a 1 T (10000 Oe) field, which is evidently out of the range in which M is linear with H. Thus, the susceptibility values are biased at low temperature, corresponding to an artificially low M/H slope, explaining the decrease of $\chi T(T)$ observed by these authors. Finally, the peak of the out of phase component $\chi''(T)$ of the ac susceptibility observed below 3 K is a proof of 3D ferromagnetic ordering, with a Curie temperature $T_C=2.7$ K deduced from the maximum of $\chi'(T)$.

Mn DL-*malate trihydrates (**12**)*: The structure of the manganese DL-malate trihydrate **12** is a 3D network of interconnected rings containing either four or two Mn^{II} atoms. Its magnetic behaviour has not been reported to date and is presented in Figure S5 in the Supporting Information. The magnetic susceptibility increases steadily with decreasing temperature, denoting a paramagnetic-like behaviour within the whole temperature range. The $\chi T(T)$ curve reaches a plateau of 4.16 $K cm^3 mol^{-1}$ between the ambient temperature and 115 K. Below, it decreases to virtually zero, denoting the existence of antiferromagnetic interactions between Mn^{II} centres. No long-range antiferromagnetic ordering was observed above 1.8 K.

Conclusion

The 12 compounds investigated in the present work include a new family of chiral carboxylate-bridged M^{II} malates. Their solvothermal synthesis, structures and magnetic properties were compared with those of other analogues, the magnetic properties of which were not or incorrectly reported previously.[31,34] The solvothermal route seems efficient for stabilising new coordination compounds. Different structural types with various dimensionalities (1D, 3D) of the magnetic network and various hydration ratios were obtained depending on whether the starting malic acid was the racemic mixture or the pure L enantiomer. Compared with the mandelic acid,[30] no racemisation was observed here. Another point arises that concerns the effect on the obtained structures of both the anion (SO_4^{2-}/Cl^-) and the metal ion chosen for the starting materials. Further investigation is needed for examining, for instance, the possible relation with the acido-basicity of the metal precursors.

Furthermore, the magnetic properties of all compounds have been analyzed in detail and interpreted on the basis of their crystal structures. Relatively few magnetic data have been reported so far on transition-metal malates and some were misinterpreted. A great variety of behaviours have

been found. As for the three new magnetic chiral compounds **1**–**3**, CD spectra in the solid state indicate a transfer of chirality from the malate to the magnetic centre. The three derivatives are antiferromagnetic, but we succeeded in the synthesis of new heterometallic analogues **5** and **6**, which show a weak ferromagnetic long-range ordering at very low temperatures ($\approx$1.8 and 2.31 K respectively), thus behaving as chiral magnets.

The magnetic properties of compounds **7**, **8**, **9** and **12** are reported for the first time. The chiral Co^{II} and Ni^{II} L-malate trihydrates are ferromagnetic 1D systems, whereas the Mn^{II} DL-malate trihydrate is a 3D antiferromagnet, without long-range ordering above 1.8 K. Finally the behaviours of the Co^{II} and Ni^{II} DL-malate dihydrates have been carefully re-investigated, showing that both are classical ferromagnets with Curie temperatures $T_C = 1.63$ K and 2.70 K respectively.

Overall, the exchange coupling does effectively go through carboxylato bridges with various geometries;[64] for example, extensive work on Cu^{II} complexes has shown that the exchange coupling is strongly antiferromagnetic with a *syn–syn* conformation,[65] very weakly so (possibly ferromagnetic[66]) with a *syn–anti* conformation[67,30] and weak-to-medium antiferromagnetic with an *anti–anti* conformation.[68] The results presented above confirm that the carboxylato bridges generally favour weak interactions and also that small structural variations may have an effect on the magnitude and the sign of the exchange coupling. It remains that α-hydroxycarboxylates are simple chiral ligands interesting for the design of chiral magnetic systems, which are still seldom in the literature. Further studies on other similar ligands are under way that might be useful for trying to solve the issue of the coupling between magnetism and chirality.

Experimental Section

General remarks: Thermogravimetric experiments were performed by using a Setaram TG92 instrument (heating rate of 5 °C min^{-1}, air stream). FT-IR studies were performed with an ATI Mattson Genesis computer-driven instrument (0.1 mm thick powder samples in KBr). UV/Vis/NIR studies were performed with a Perkin–Elmer Lambda 19 instrument (spectra recorded by reflection with a resolution of 4 nm and a sampling rate of 480 nm min^{-1}). Elemental analysis was performed by using a Thermo_Finnigan EA 1112 setup (Service d'analyses, ICS, Strasbourg, France).

Magnetic studies were carried out by using a Quantum Design SQUID MPMS-XL magnetometer (±5 T, 1.8–300 K) on several sets of crystal or powder samples. Specific heat measurements were done by using a quasi-adiabatic method.[69]

L-Malate monohydrate compounds 1–6: Compounds **1** (pink crystals, yield: 0.70 g, 73% based on the metal salt), **2** (pale green crystals, yield: 0.57 g, 59%), **3** (pink blue crystals, yield: 0.53 g, 54%), **4** (white crystals, yield: 0.39 g, 39%), **5** (dark pink crystals) and **6** (yellow crystals) were synthesised by the hydrothermal method from $MnCl_2{\cdot}4H_2O$ (99% Fluka; 0.922 g, 4.66 mmol), $FeCl_2{\cdot}6H_2O$ (99% Fluka; 1.094 g, 4.66 mmol), $Co(SO_4){\cdot}7H_2O$ (98% Acros; 1.309 g, 4.66 mmol), $ZnCl_2$ (98% Fluka; 1.094 g, 4.66 mmol) and equimolar mixtures of $MnCl_2{\cdot}4H_2O$ (0.461 g, 2.33 mmol) and $Co(SO_4){\cdot}7H_2O$ (0.655 g, 2.33 mmol) or $NiCl_2{\cdot}6H_2O$ (99.99% Sigma; 0.554 g, 2.33 mmol), respectively, and L-malic acid (99% Acros; 0.937 g, 6.99 mmol), KOH (Merck) (0.523 g, 9.32 mmol) in water/ethanol (5 mL, 50:50 v/v). The starting mixtures were transferred to sealed Teflon lined hydrothermal bombs (bomb volume: 23 mL) and heated at 180 °C for 2 days under autogenous pressure. After cooling in a water bath, the resulting compounds were washed and rinsed with distilled water and absolute ethanol. Elemental analyses, IR and UV data for the series of compounds are given in the Supporting Information.

L-Malate trihydrate compounds 7,[38] 8[39] and 9: Compounds **7** (pink blue crystals , yield: 0.73 g, 64%), **8** (green crystals, yield: 0.90 g, 79%), **9** (dark pink crystals) were synthesised similarly from $CoCl_2{\cdot}6H_2O$ (98% Acros; 1.108 g, 4.66 mmol), $NiCl_2{\cdot}6H_2O$ (99.99% Sigma; 1.107 g, 4.66 mmol) and from $CoCl_2{\cdot}6H_2O$ (98% Acros; 0.554 g, 2.33 mmol) and $NiCl_2{\cdot}6H_2O$ (99.99% Sigma; 0.554 g, 2.33 mmol), respectively. Elemental analyses, IR and UV data for the series of compounds are given in the Supporting Information.

DL-Malate dihydrates 10 and 11:[31] Compounds **10** (pink blue crystals, yield: 0.65 g, 61%) and **11** (green crystals, yield: 0.68 g, 64%) were synthesised similarly as above starting from $CoCl_2{\cdot}6H_2O$ (98% Acros; 1.108 g, 4.66 mmol) and $NiCl_2{\cdot}6H_2O$ (99.99% Sigma; 1.108 g, 4.66 mmol) with DL-malic acid (99+% Acros; 0.937 g, 6.99 mmol). Elemental analyses, IR and UV data for the series of compounds are given in the Supporting Information.

DL-Malate trihydrate (12):[35] Compound **12** (pink crystals, yield: 0.39 g, 35%) was synthesised in the same manner as above from $[MnCl_2{\cdot}4H_2O]$ (99% Fluka; 0.922 g, 4.66 mmol) and DL-malic acid (99+% Acros; 0.937 g, 6.99 mmol). Elemental analyses, IR and UV data are given in the Supporting Information.

X-ray crystallographic study: Single crystals of transition-metal malates **1**–**12** were mounted on a Nonius Kappa-CCD area detector diffractometer ($Mo_{K\alpha}$, $\lambda = 0.71073$ Å). The complete conditions of data collection (Denzo software) and structure refinements are given below. The cell parameters were determined from reflections taken from one set of 10 frames (1.0° steps in phi angle), each at 20 s exposure. The structures were solved by using direct methods (SHELXS97) and refined against F^2 using the SHELXL97 software.[70] All non-hydrogen atoms were refined anisotropically. Hydrogen atoms were generated according to stereochemistry and refined using a riding model in SHELXL97. CCDC 283387–283395 contain the supplementary crystallographic data for this paper. These data can be obtained free of charge from The Cambridge Crystallographic Data Centre via www.ccdc.cam.ac.uk/data_request/cif.

The details of crystal data recording and refinement are given in the Supporting Information (Tables S4–S6).

Acknowledgement

This is part of the Ph.D. thesis work of one of us (A.B.). We thank Alain Derory, Didier Burger and Jeannot Stoll from Institut de Physique et Chimie des Matériaux de Strasbourg, Strasbourg (France), for their contribution to magnetic measurements, thermogravimetric measurements and fabrication of Teflon lined bombs. We thank the CNRS, the Université Louis Pasteur de Strasbourg and the European Community (European Network of Excellence MAGMANet, Sixth Framework programme—Priority [3-NMP], Proposal/Contract #: 515767-2) for funding to P.R. and G.R.

[1] R. C. Mehrotra, R. Bohra, *Metal Carboxylates*, Academic Press, New York, **1983**.

[2] C. N. R. Rao, S. Natarajan, R. Vaidhyanathan, *Angew. Chem.* **2004**, *116*, 1490–1521; *Angew. Chem. Int. Ed.* **2004**, *43*, 1466–1496, and references therein.

[3] *Catalysis in Organic Synthesis* (Ed.: W. H. Jones), Academic Press, New York, **1980**.

[4] R. A. Sheldon, J. K. Kochi, *Metal-Catalyzed Oxidations of Organic Compounds*, Academic Press, New York, **1981**.
[5] P.-G. Lassahn, V. Lozan, G. A. Timco, P. Christian, C. Janiak, R. E. P. Winpenny, *J. Catal.* **2004**, *222*, 260–267.
[6] E. D. Park, Y.-S. Hwang, J. S. Lee, *Catal. Commun.* **2001**, *2*, 187–190.
[7] T. Szymanska-Buzar, J. J. Ziolkowski, *J. Mol. Catal.* **1981**, *11*, 371–381.
[8] O. A. Yaghi, M. O'Keeffe, N. W. Ockwig, H. K. Chae, M. Eddaoudi, J. Kim, *Nature* **2003**, *423*, 705–714.
[9] G. Férey, C. Mellot-Draznieks, C. Serre, F. Millange, J. Dutour, S. Surblé, I. Margiolaki, *Science* **2005**, *309*, 2040–2042.
[10] S. R. Halper, S. M. Cohen, *Inorg. Chem.* **2005**, *44*, 486–488.
[11] C. D. Wu, A. Hu, L. Zhang, W. Lin, *J. Am. Chem. Soc.* **2005**, *127*, 8940–8941.
[12] Y. Rodriguez-Martín, C. Ruiz-Perez, J. Sanchiz, F. Lloret, M. Julve, *Inorg. Chim. Acta* **2001**, *318*, 159–165.
[13] S. O. H. Gutschke, D. J. Price, A. K. Powell, P. T. Wood, *Angew. Chem.* **2001**, *113*, 1974–1977; *Angew. Chem. Int. Ed.* **2001**, *40*, 1920–1923.
[14] M. Riou-Cavellec, C. Albinet, C. Livage, N. Guillou, M. Noguèse, J. M. Grenèche, G. Férey, *Solid State Sci.* **2002**, *4*, 267–270.
[15] M. J. Plater, M. R. S. J. Foremen, R. A Howie, J. M. S. Skakle, A. M. Z. Slawin, *Inorg. Chim. Acta* **2001**, *315*, 126–132.
[16] G. Blay, I. Fernandez, T. Gimenez, J. R. Pedro, R. Ruiz, E. Pardo, F. Lloret, M. C. Munoz, *Chem. Commun.* **2001**, 2102–2103.
[17] R. Clément, S. Decurtins, M. Gruselle, C. Train in *Molecular Magnets Recent Highlights* (Eds.: W. Linert, M. Verdaguer), Springer, New-York, **2003**.
[18] R. Sessoli, D. Gatteschi, A. Caneschi, M. Novak, *Nature* **1993**, *365*, 149.
[19] F. S. Delgado, N. Kerbellec, C. Ruiz-Pérez, J. Cano, F. Lloret, M. Julve, *Inorg. Chem.* **2006**, *45*, 1012–1020.
[20] H. Kumagai, K. Inoue, *Angew. Chem.* **1999**, *111*, 1694–1696; *Angew. Chem. Int. Ed.* **1999**, *38*, 1601–1603.
[21] L. D. Barron, *Nature* **2000**, *405*, 895–896.
[22] G. L. J. A. Rikken, E. Raupach, *Nature* **2000**, *405*, 932–935.
[23] M. Minguet, D. Luneau, E. Lhotel, V. Villar, C. Paulsen, D. B. Amabilino, J. Veciana, *Angew. Chem.* **2002**, *114*, 606–609; *Angew. Chem. Int. Ed.* **2002**, *41*, 586–589.
[24] P. Gerbier, N. Domingo, J. Gomez-Segura, D. Ruiz-Molina, D. B. Amabilino, J. Tejada, B. E. Williamson, J. Veciana, *J. Mater. Chem.* **2004**, *14*, 2455–2460.
[25] N. S. Ovanesyan, V. D. Makhaev, S. M. Aldoshin, P. Gredin, K. Boubekeur, C. Train, M. Gruselle, *Dalton Trans.* **2005**, 3101–3107.
[26] R. Carballo, A. Castiñieras, S. Balboa, B. Covelo, J. Niclós, *Polyhedron* **2002**, *21*, 2811–2818.
[27] R. Carballo, B. Covelo, S. Balboa, A. Castiñieras, J. Niclós, *Z. Anorg. Allg. Chem.* **2001**, *627*, 948–954.
[28] D. A. House, J. Browning, J. R. Pipal, W. T. Robinson, *Inorg. Chim. Acta* **1999**, *292*, 73–83.
[29] I. K. Smatanova, J. Marek, P. Svancarek, P. Schwendt, *Acta Crystallogr. Sect. C* **2000**, *56*, 154.
[30] A. Beghidja, S. Hallynck, R. Welter, P. Rabu, *Eur. J. Inorg. Chem.* **2005**, 662–669.
[31] F.-T. Xie, L.-M. Duan, J.-Q. Xu, L. Ye, Y.-B. Liu, X.-X. Hu, J.-F. Song, *Eur. J. Inorg. Chem.* **2004**, 4375–4379.
[32] F. E. Mabbs, D. J. Machin, *Magnetism and Transition Metal Complexes*, Chapman and Hall, London, **1973**.
[33] O. Kahn, *Molecular Magnetism*, VCH, Weinheim, **1993**.
[34] Y. Guo, D. Xiao, E. Wang, Y. Lu, J. Lü, X. Xu, L. Xu, *J. Solid State Chem.* **2005**, *178*, 776–781.
[35] A. T. H. Lenstra, J. Diller, *Bull. Soc. Chim. Belges* **1983**, *92*, 257–262.
[36] M. Fleck, E. Tillmanns, L. Bohaty, *Z. Kristallogr.* **2001**, *216*, 633–645.
[37] A. Karipides, A. Thomas Reed, *Inorg. Chem.* **1976**, *15*, 44–47.
[38] L. Kryger, S. E. Rasmussen, *Acta Chem. Scand.* **1972**, *26*, 2349–2359.
[39] Z. H. Zhou, J.-J. Ye, Y.-F. Deng, G. Wang, J.-X. Gao, H.-L. Wan, *Polyhedron* **2002**, *21*, 787–790.
[40] W. Van Havere, A. T. H. Lenstra, H. J. Geise, *Acta Crystallogr. Sect. B* **1980**, *36*, 3117–3120.
[41] K. Nakamoto, *Infrared and Raman Spectra of Organic and Coordination Compounds*, 4th ed., Wiley-Interscience, New York, **1986**, p. 231.
[42] A. B. P. Lever, *Inorganic Electronic Spectroscopy*, 2nd ed., Elsevier, Amsterdam **1984**.
[43] L. Banci, A. Bencini, C. Benelli, D. Gatteschi, C. Zanchini, *Struct. Bonding (Berlin)* **1982**, *52*, 37.
[44] Y. S. Dou, *J. Chem. Educ.* **1990**, *67*, 134.
[45] M. Minguet, D. B. Amabilino, K. Wurtz, J. Veciana, *J. Chem. Soc. Perkin Trans. 2* **2001**, *2*, 670–676.
[46] R. L. Carlin, *Magnetochemistry*, Springer, Berlin, **1986**.
[47] M. Drillon, J. C. Gianduzzo, R. Georges, *Phys. Lett. A* **1983**, *96*, 413.
[48] M. Verdaguer, A. Gleizes, J.-P. Renard, J. Seiden, *Phys. Rev. B* **1984**, *29*, 5144–5155.
[49] M. Drillon, E. Coronado, R. Georges, J. C. Gianduzzo, J. Curely, *Phys. Rev. B* **1989**, *40*, 10992–10998.
[50] A. Gleizes, M. Verdaguer, *J. Am. Chem. Soc.* **1984**, *106*, 3727–3737.
[51] R. Clément, A. Léaustic in *Magnetism: Molecules to Materials, Vol. II* (Eds.: J. S. Miller, M. Drillon), Wiley-VCH, Weinheim, **2001**, pp. 397–423.
[52] J.-M. Rueff, N. Masciocchi, P. Rabu, A. Sironi, A. Skoulios, *Chem. Eur. J.* **2002**, *8*, 1813–1820.
[53] D. Ghoshal, G. Mostafa, T. K. Maji, E. Zangrando, T.-H. Lu, J. Ribas, N. R. Chaudhuri, *New J. Chem.* **2004**, *28*, 1204–1213.
[54] P. Rabu, J.-M. Rueff, Z.-L. Huang, S. Angelov, J. Souletie, M. Drillon, *Polyhedron* **2001**, *20*, 1677–1685.
[55] J. Souletie, M. Drillon, P. Rabu, S. K. Pati, *Phys. Rev. B* **2004**, *70*, 054410.
[56] J. Souletie, M. Drillon, P. Rabu in *Magnetism: Molecules to Materials, Vol. V* (Eds.: J. S. Miller, M. Drillon), Wiley-VCH, Weinheim, **2005**, pp. 347–377.
[57] P. Rabu, J.-M. Rueff, Z.-L. Huang, S. Angelov, J. Souletie, M. Drillon, *Polyhedron* **2001**, *20*, 1677–1685.
[58] J. Souletie, *J. Phys. (Paris)* **1988**, *49*, 1211–1217.
[59] J. Souletie, P. Rabu, M. Drillon, *Phys. Rev. B* **2005**, *72*, 214427.
[60] J.-M. Rueff, S. Pillet, N. Claiser, G. Bonaventure, M. Souhassou, P. Rabu, *Eur. J. Inorg. Chem.* **2002**, 895–900.
[61] O. Castillo, A. Luque, P. Romá, F. Lloret, M. Julve, *Inorg. Chem.* **2001**, *40*, 5526–5535.
[62] *Research Frontiers in Magnetochemistry* (Ed.: C. J. O'Connor), World Scientific Publishers, **1993**.
[63] G. A. Baker, G. S. Rushbrooke, H. E. Gilbert, *Phys. Rev.* **1964**, *135*, A1272.
[64] E. Colacio, J. M. Dominguez-Vera, J. P. Costes, R. Kivekäs, J. P. Laurent, J. Ruiz, M. Sundberg, *Inorg. Chem.* **1992**, *31*, 774–778.
[65] B. N. Figgis, R. L. Martin, *J. Chem. Soc.* **1956**, 3837–3846.
[66] D. K. Toxle, S. K. Hoffmann, W. E. Hatfield, P. Singh, P. Chaudhuri, *Inorg. Chem.* **1988**, *27*, 394–399.
[67] R. L. Carlin, K. Kopinga, O. Kahn, M. Verdaguer, *Inorg. Chem.* **1986**, *25*, 1786–1789.
[68] M. Kato, Y. Muto, *Coord. Chem. Rev.* **1988**, *92*, 45–83.
[69] The calorimeter was designed by R. Kuentzler and Y. Dossmann (Strasbourg) for measurement in temperature range 1.6–40 K. It contained an adiabatic chamber with a sapphire sample holder, equipped with a Ge resistance thermometer and an evaporation deposit Cr/Ti heater. The sample holder was suspended with nylon threads. The accuracy of the measurement was better than 1%.
[70] G. M. Sheldrick, SHELXL-97, University of Göttingen, Göttingen (Germany), **1997**.

Received: January 3, 2006
Published online: July 26, 2006

